First-principles study of the linear electro-optical response in strained SrTiO_{3}

Ali K. Hamze and Alexander A. Demkov

First principles study of the linear electro-optical response in strained SrTiO₃

Ali K. Hamze[1] and Alexander A. Demkov[1*]

[1]Department of Physics, The University of Texas at Austin, Austin, TX, 78712, USA

Abstract

We report a density functional theory study of the Pockels effect (linear electro-optical effect) in epitaxially strained SrTiO₃. The electro-optical response is calculated for biaxial strain values ranging from -2.0% to 2.0% relative to the theoretically-optimized lattice constant. Under 1.0% tensile strain, the Pockels tensor components increase dramatically, with the largest components reaching maximum values of $r_{111} = r_{222} = 505.64$ pm/V. Under 1.2% compressive strain, the Pockels tensor exhibits a similarly large peak with a maximum value of $r_{333} = 236.55$ pm/V. These peaks in the electro-optical response originate from the softening of the phonon modes associated with ferroelectric phase transitions that result in the loss of inversion symmetry. Our results suggest that under the right circumstances, SrTiO₃ can yield a very large electro-optical response, comparable to that of BaTiO₃, which has one of the largest known responses.

Introduction

Silicon photonics has attracted a great deal of attention in recent years due to its potential for low-cost, low-power devices with very high data transmission rates [1–5]. The need for such devices is particularly urgent in conventional electronics as copper interconnects used today become unviable at signal frequencies above 40 GHz, a frequency that inter-chip communication is expected to reach this year [6]. Though optical modulators and switches have been developed for silicon photonics using the plasma-dispersion effect in silicon, they suffer from insertion losses, high power consumption, and undesired intensity modulations [1,7,8]. Hybrid, transition metal oxide-based devices have the potential to mitigate these problems as they offer access to optical phenomena not available in pure silicon, such as the linear electro-optic (EO) (or Pockels) effect. The Pockels effect, which is a change in the refractive index of a material upon the application of an electric field, exists only in materials with no inversion symmetry. Silicon is centrosymmetric and therefore has to be strained to show even a weak EO response [9,10]. As a result, there are currently very few silicon photonic devices exploiting the Pockels effect [11,12]. Materials with a large Pockels effect are well-suited for low-power and high-speed optical modulation [13]. In the telecommunications industry, LiNbO₃ has long been used as the material of choice for optical modulators due to its sizable Pockels coefficient of ~30 pm/V [13–16], which makes it potentially attractive in silicon photonic applications. However, LiNbO₃ cannot be easily integrated on silicon, which has inspired a search for materials with large Pockels coefficients that can be [13,17].

The most promising among these materials is the ferroelectric perovskite BaTiO₃ (BTO), which exhibits one of the largest known Pockels coefficients—both in thin films and in bulk (which has a coefficient of order ~1600 pm/V [16])—due to its lack of inversion symmetry and the presence

*demkov@physics.utexas.edu

of soft phonon modes [18,19]. BTO can be also be grown epitaxially on silicon (001) [20,21]. As a result, BTO epitaxially integrated on silicon for use in photonics has been the subject of extensive, but primarily experimental, study [7,12,13,17,19,22,23].

Finding other electro-optically active materials that can be integrated on silicon is of significant scientific interest and of practical importance, as doing so will allow for greater flexibility in device design and applications. The incipient ferroelectric $SrTiO_3$ (STO) is in many respects similar to BTO, but it is cubic at room temperature, and therefore, by symmetry, the Pockels effect is forbidden. However, STO is extremely close to a ferroelectric (FE) phase transition. Below 105 K, STO undergoes a structural phase transition to a tetragonal, non-polar antiferrodistortive (AFD) phase [24–26]. The dielectric properties are not significantly affected by this phase transition. Upon further cooling, the dielectric constant obeys a Curie-Weiss law that suggests a phase transition at a Curie temperature of ~20 K [27–29]. No phase transition occurs, however. Instead, the paraelectric phase is stabilized by quantum fluctuations [30–33]. The dielectric constant continues to increase as the temperature is lowered until it saturates to a constant value of ~20,000 at 4 K and below [29,30]. Additionally, like BTO, epitaxial thin films of STO can be grown on silicon [20,34–41], making it a candidate for integration into silicon photonic devices. Under epitaxial strain, phases previously forbidden for bulk crystals can appear [42]. Indeed, in STO, a FE phase stabilizes under biaxial strain [31,32,43,44]. This in turn, breaks the inversion symmetry of the unit cell, which should allow for an EO response. When grown on silicon (001), STO is placed under biaxial, compressive strain of -1.5% [35]. Therefore, one would expect a non-zero EO response under these conditions. Indeed, a non-zero EO response has been seen experimentally in strained STO, but not when grown on silicon. Ma *et al* [45] grew STO on (110)-oriented $DyScO_3$, which led to fixed, non-uniform, in-plane strains of 1.1% and 1.2%. Furthermore, strained STO has been studied using density functional theory by Antons *et al*. [43], who predicted a divergence in the dielectric constant for certain critical values of both compressive and tensile strain. This divergence in the dielectric constant is driven by the softening of phonon modes at critical strain values at the onset of the second-order structural phase transition [43]. This was also observed theoretically and experimentally by Peng *et al*. [46], who studied thin films of STO under compressive, in-plane strain.

In this paper, we investigate theoretically the electro-optical response of STO as a function of epitaxial strain. Using density functional theory, we vary the in-plane strain of bulk STO and allow the *c*-axis to respond. We are interested in modeling room-temperature STO because a device is likely to run at room temperature. Therefore, we do not include the AFD rotations of the oxygen octahedra because they are not present in the stable phases of the crystal at this temperature, which are the ferroelectric tetragonal, high temperature tetragonal and ferroelectric orthorhombic phases (FTI, HT and FOI, respectively), as shown by Pertsev et al. [31,32]. We then study the influence of strain on the EO (Pockels) tensor. Moreover, we investigate the origin of the large EO response at the critical strain values and trace it to a strain-driven structural phase

transition caused by mode softening. A simple phenomenological model is invoked to highlight the physics of the phenomenon.

Background and Methods

The Pockels tensor, also called the linear electro-optic (EO) tensor, relates the change in the inverse dielectric tensor to an external electric field [16]:

$$\Delta(\epsilon^{-1})_{ij} = \sum_k r_{ijk} E_k. \tag{1}$$

Because the change is linear in the electric field, centrosymmetric crystals do not exhibit the Pockels effect. There are three contributions to the Pockels tensor: an electronic contribution from the valence electrons, an ionic contribution from the displacement of the ions, and a piezoelectric contribution from the distortion of the unit cell through the converse piezoelectric effect [18,47]. Following Veithen *et al* [47], these can be calculated by expanding the electric enthalpy to third order in the applied electric field. The dielectric tensor can be calculated in terms of the second derivative with respect to the applied external electric field. The details of how this is done in ABINIT can be found in [48,49]. As a test, we computed the dielectric constants for purely ionic NaCl and the simple mixed-bonding binary oxide α-quartz. At the theoretically-optimized lattice constants, we find the dielectric constants of these materials to be 5.24 and 4.86, respectively, in fair agreement with the experimental values of 5.90 [50] and 4.65 [51]. The Pockels tensor can then be found from inverting the total derivative of the dielectric tensor. The electronic contribution comes from the valence electrons, and (in the principal axes of the crystal) can be written in terms of the second order nonlinear susceptibility $\chi_{ijk}^{(2)}$ as

$$r_{ijk}^{\text{el}} = -\frac{8\pi}{n_i^2 n_j^2} \chi_{ijl}^{(2)} \bigg|_{l=k}, \tag{2}$$

where the n_i are the principal indices of refraction [18,47]. The ionic contribution comes from relaxation of the ions in the presence of the external electric field, and can be written in terms of a sum over transverse optical phonon modes at the Γ point of the Brillouin zone [47]. This is given by

$$r_{ijk}^{\text{ion}} = -\frac{4\pi}{\sqrt{\Omega_0} n_i^2 n_j^2} \sum_m \frac{\alpha_{ij}^m p_{m,k}}{\omega_m^2}. \tag{3}$$

Here, Ω_0 is the volume of the unit cell, α_{ij}^m is the Raman susceptibility, $p_{m,k}$ is the mode polarity, and ω_m is the frequency of the mode m. The Raman susceptibility and mode polarity are in turn given by

$$\alpha_{ij}^m = \sqrt{\Omega_0} \sum_{\kappa,\beta} \frac{\partial \chi_{ij}^{(1)}}{\partial \tau_{\kappa,\beta}} u_m(\kappa\beta), \tag{4}$$

$$p_{m,k} = \sum_{\kappa,\beta} Z_{\kappa,k\beta}^* u_m(\kappa\beta), \tag{5}$$

where $u_m(\kappa\beta)$ is the transverse optic phonon eigendisplacement[1] of atom κ in the direction β at Γ due to mode m, $\tau_{\kappa,\beta}$ is the actual displacement of atom κ in the direction β, $\chi_{ij}^{(1)}$ is the linear dielectric susceptibility, and $Z_{\kappa,k\beta}^*$ is the Born effective charge of atom κ. The sum of the electronic and ionic contributions constitutes the *clamped* (strain-free) EO tensor $r_{ijk}^{\eta} = r_{ijk}^{\text{el}} + r_{ijk}^{\text{ion}}$. The *unclamped* (stress-free) EO tensor r_{ijk}^{σ} includes the piezoelectric contribution, and can be written in terms of the elasto-optic (photoelastic) coefficients $p_{ij\mu\nu}$ and the piezoelectric strain coefficients $d_{k\mu\nu}$ [47] as

$$r_{ijk}^{\sigma} = r_{ijk}^{\eta} + \textstyle\sum_{\mu,\nu=1}^3 p_{ij\mu\nu}d_{k\mu\nu}. \tag{6}$$

In our calculations, we neglect the piezoelectric contribution because its contribution to the EO tensor is small (see Discussion for details). We calculate the EO tensor using density functional theory (DFT) and density functional perturbation theory (DFPT). Our calculations were done using the ABINIT software package [47–49,52–55] with Teter norm-conserving pseudopotentials [56]. The valence electron configurations were $4s^2 4p^6 5s^2$ for the strontium atom (where we have included the semi-core s and p electrons), $3s^2 3p^6 4s^2 3d^2$ for the titanium atom, and $2s^2 2p^4$ for the oxygen atoms. The exchange-correlation energy was calculated in the local density approximation (LDA) [57,58]. We use a plane-wave cut off energy of 50 Hartree and a 12x12x12 Monkhorst-Pack k-point grid [59] for all calculations. All cells were relaxed until the interatomic forces were smaller than 2×10^{-7} Hartree/Bohr. A theoretically-optimized lattice constant of $a_{\text{STO}} = 3.845$ Å $= 7.266$ Bohr was used for the zero-strain case, which agrees well with the experimental value of 3.90 Å $= 7.37$ Bohr [60] (while slightly underestimating it, as is typical for LDA calculations). For the strained systems, the in-plane lattice constants were changed from the zero-strain value according to the amount of strain and were fixed, after which the c-axis lattice constant was optimized. Tetragonal symmetry of the cell was maintained in order to model an epitaxial film. Strains in the range ±2% were considered. After the cells were optimized, DFPT was used to calculate the phonons, Born effective charges, and dielectric tensor [49]. DFPT was also used in conjunction with the $2n + 1$ theorem to calculate the nonlinear responses $\chi_{ijl}^{(2)}$ and $\partial\chi_{ij}^{(1)}/\partial\tau_{\kappa,\beta}$ [47]. These can then be combined as discussed above to calculate the EO tensor. It is necessary to calculate the elasto-optic tensor to calculate the piezoelectric contribution to the EO response, but ABINIT does not calculate it natively. To calculate it, we write it in terms of the strain as [61]

$$\Delta(\epsilon^{-1})_{ij}^{\text{piezo}} = \textstyle\sum_{\mu,\nu=1}^3 p_{ij\mu\nu}e_{\mu\nu}, \tag{7}$$

where $e_{\mu\nu}$ is the strain tensor. We can do this because the strain can be written as $e_{\mu\nu} = d_{k\mu\nu}E_k + s_{ij\mu\nu}\sigma_{\mu\nu}$, where $d_{k\mu\nu}$ is the piezoelectric tensor, E_k is the applied electric field, $s_{ij\mu\nu}$ is the compliance tensor, and $\sigma_{\mu\nu}$ is the stress tensor. Since the piezoelectric contribution is only

---

[1] The eigendisplacement $u_m(\kappa\beta)$ is related to the more typically used phonon eigenvectors by $u_m(\kappa\beta) = \gamma_m(\kappa\beta)/\sqrt{M_\kappa}$, where M_κ is the mass of atom κ.

possible when we consider stress-free boundary conditions, the second term vanishes and Equation (7) reduces to the piezoelectric contribution we see when Equation (6) is inserted into Equation (1). Writing it in this way enables us to calculate the elasto-optic tensor components as described in [62] by selectively straining the unit cell, calculating the dielectric tensor, inverting it, and taking a numerical derivative. We used strains of ±0.0025% for the diagonal elements of the strain tensor and rotations of the lattice vectors of 0.45° for the off-diagonal elements of the strain tensor in calculating the numerical derivative.

As will be discussed below, anharmonicity in the crystal is the primary driver of the EO response. To quantify the anharmonicity, mode Grüneisen parameters were calculated for several selected strain values. For an isotropic material, the mode Grüneisen parameter for phonon mode i and k-point q is defined as [63]

$$\gamma_i(\boldsymbol{q}) = -\frac{V}{\omega_i(\boldsymbol{q})}\frac{\partial \omega_i(\boldsymbol{q})}{\partial V},\tag{8}$$

where V is the volume of the cell and $\omega_i(\boldsymbol{q})$ is the frequency of the mode at $\boldsymbol{q}$. For an anisotropic material, this can be generalized and written in terms of the strain e_{jk} as

$$\gamma_{jk}^{i,P}(\boldsymbol{q}) = -\frac{1}{\omega_{i,P}(\boldsymbol{q})}\frac{\partial \omega_{i,P}(\boldsymbol{q})}{e_{jk}},\tag{9}$$

where the index P labels the polarization of the phonon mode [64]. These calculations were done using ABINIT in the same manner as the electro-optical calculations described above. To calculate the Grüneisen parameters for a given biaxial strain in the isotropic approximation, we need the phonon frequencies as a function of volume at that strain. Therefore, we apply additional hydrostatic strain to the already biaxially-strained crystal and calculate the phonon spectrum at the Γ point (because only the phonons at Γ contribute to the EO tensor). We then have phonon spectrum as a function of volume, from which we can extract the Grüneisen parameters using the finite difference method and Equation (8). Similarly, for the anisotropic model, we apply additional strain to the biaxially strained crystal to find the frequency as a function of that strain component, which we can then use to calculate the corresponding component of the anisotropic Grüneisen tensor with the finite difference method and Equation (9). Finally, the symmetry of the crystal will reduce the number of independent components of the Grüneisen tensor, reducing the total number of calculations necessary to compute the full tensor.

For the rest of this paper we use Voight notation [16] for the first two indices of the EO tensor. That is to say, the index i in r_{ij} is a Voight index labeling which component of the inverse dielectric tensor is responding to the perturbing optical electric field and j labels the component of the field.

Results and Discussion

Before we discuss our predictions for the EO tensor, let us briefly remark on the phase transitions we observe when biaxial (epitaxial) strain is applied to STO. In Figure 1, we plot the

polarization of the cell as a function of strain. Under compressive strain beyond -1.2%, the titanium atom is displaced in the (001) direction and the crystal undergoes a FE phase transition to a non-centrosymmetric, tetragonal $P4mm$ phase from the centrosymmetric, tetragonal $P4/mmm$ phase seen between -1.2% strain and 1.0% strain (except at 0.0% strain, where we have the cubic perovskite $Pm\bar{3}m$ phase). For tensile strain above 1.0%, the titanium and strontium ions are displaced in the (110) direction. The space group becomes $Amm2$, and we have an orthorhombic, non-centrosymmetric structure. These results are in qualitative agreement with the findings of Antons $et\ al.$ [43]. There is, however, one notable difference: we predict larger magnitudes of the critical strains at which the phase transitions occur. The difference in critical strains is likely due to the different pseudopotentials used in our respective calculations. The critical values of strain, at which the FE phase transitions occur, are also much larger than predicted using a Landau-Ginzburg-Devonshire model [31,32]. As discussed by Antons $et\ al$, this is likely due to the underestimation of the lattice constant in LDA, which stabilizes the paraelectric phase [43,65]. Another possible influence on the critical strain values is the absence of rotations of the oxygen octahedra in our analysis. The onset of these phase transitions is driven by softening phonon modes, as also observed by Antons $et\ al.$ [43]. A plot of the frequency of the first optical mode as a function of the in-plane strain is shown in Figure 2. For compressive strain, the first optical phonon mode displaces the titanium ion in the (001) direction. For tensile strain below the critical value, the first optical mode is actually a double-degenerate mode, which displaces the titanium ion in the $(\bar{1}10)$ and $(\overline{11}0)$ directions. For tensile strain above the critical value, the degeneracy is lifted and the softest mode is the mode which displaces the titanium atom in the $(\bar{1}10)$ direction. The displacement patterns of these phonon modes are shown in Figure 3.

Our predictions of the magnitudes of the clamped EO tensor components under compressive and tensile strain are shown in Figures 4 and 5, respectively. Again, there is no EO response without strain because the unstrained unit cell is centrosymmetric. For compressive strain, we predict a large spike in the r_{33} component of the EO tensor, with a maximum of $r_{33} = 236.55$ pm/V at -1.20% strain. There is also a peak in $r_{13} = r_{23}$ at this strain with a maximum value of $r_{13} = 50.22$ pm/V. These large responses would result from an electric field which displaces the atoms parallel to the softening phonon mode, the displacement pattern of which is shown in Figure 3(a). On the other hand, r_{42} remains relatively small and increases slowly with strain. This is in contrast to BTO, where the largest component under compressive strain is r_{42} (which is also the case under no strain for BTO [19,66]). This difference is likely due to how STO and BTO polarize under compressive strain. In STO, the polarization is entirely in the (001) direction, while in BTO, the polarization is closer to (111). The phonon that contributes most to the EO response goes very soft at this strain, with a frequency of 18.30 cm^{-1}.

For tensile strain, we predict a maximum in the EO response at 1.00% strain. The magnitude of the largest component is $r_{11} = r_{22} = 505.64$ pm/V. The magnitudes of three other components, r_{12}, r_{31}, and r_{61}, also peak at this strain, although their maximum value is below 100 pm/V.

6

Under tensile strain, the titanium atom is displaced in the [110] direction. In contrast with the compressive strain case, there are two softening phonon modes with significant contributions to the Pockels tensor. For strains smaller than the critical strain, the crystal is in the centrosymmetric, tetragonal $P4/mmm$ phase. The two softest optical modes are degenerate and displace the titanium ion in the $(\bar{1}10)$ and $(\bar{1}\bar{1}0)$ directions. The $(\bar{1}10)$ mode's primary contributions are to the r_{i1} components of the Pockels tensor, and the $(\bar{1}\bar{1}0)$ mode's primary contributions are to the r_{i2} components. Furthermore, their contributions have the same sign. For strains above the critical strain, the crystal changes to the orthorhombic $Amm2$ phase, and the degeneracy between these two softest modes is lifted. The softest mode is the mode which displaces the titanium atom in the $(\bar{1}10)$ direction. In this phase, the contributions of the modes to the Pockels tensor change. The signs of the largest contributions of the two softest modes agree for r_{11} and r_{22} and disagree for $r_{12} = r_{21}$. That two modes have nearly equal contributions to the Pockels tensor (where they agree in sign) explains why the magnitude of the largest response under tensile strain is approximately double the magnitude of the largest response under compressive strain. However, because the degeneracy is lifted, the contributions to $r_{12} = r_{21}$ don't cancel out exactly, so they therefore remain non-zero. Finally, at and above the critical strain, the contributions to $r_{31} = r_{32}$, r_{61}, and r_{62} are almost entirely due to the second softest mode, which displaces the atoms along the $(\bar{1}\bar{1}0)$ direction. In general, under tensile strain, the largest responses are those to an electric field polarized in the (100) or (010) directions. At the critical strain, the frequency of the softest mode is 16.14 cm⁻¹, and the frequency of the second softest mode is 24.33 cm⁻¹. The displacement pattern of the softest mode is shown in Figure 3(b).

In Table 1, we compare the magnitude of the piezoelectric contribution to the EO tensor to the magnitude of the clamped EO tensor at -1.0% and -1.2% strain. We see that the piezoelectric contribution is only 7.6% and 12.2% of the magnitude of the clamped tensor at these strains, respectively, justifying neglecting the piezoelectric contribution.

Our results predict responses larger than what Ma *et al* [45] measured, even for what are ostensibly similar tensile strains. Recall, however, that LDA underestimates the lattice constant and that DFT calculations are done at 0 K, making direct comparison to experimental systems difficult. However, our results suggest there are values of strain for a real STO crystal at which the EO response could indeed be quite large.

The electronic contributions to the EO tensor in STO are extremely small compared to the ionic contributions (less than 1% of the total response). As the phonon mode that leads to the FE transition softens, the ionic contribution to the EO tensor increases due to the factor of ω_m^{-2}, as can be seen in Equation (3). Furthermore, the softening mode indicates that the anharmonicity of the film, which originates from the hybridization in the titanium-oxygen bond [65], is increasing. This can be quantified in several ways. In Tables 2 and 3, we list the anisotropic Grüneisen tensor components and the isotropic Grüneisen parameter, respectively, of the first optical mode (which drives the FE phase transition) of the crystal under compressive strain. Due to the

7

tetragonal symmetry of STO under compressive strain, the only non-zero components of the anisotropic Grüneisen tensor are $\gamma_{11} = \gamma_{22}$ and γ_{33}. Recall that under compressive strain the phonon mode that goes soft and drives the divergence in the Pockels tensor is polarized along the (001)-direction. This is reflected in Table 2 in the anisotropic Grüneisen tensor: γ_{33} is positive and much larger than γ_{11}. In other words, the crystal is much more anharmonic in the (001)-direction than it is in the (100)- or (010)-directions. Furthermore, the Grüneisen parameter is significantly larger at the critical strain than at -1.0% strain. For comparison, we calculate the Grüneisen parameter of the cubic, 0.0% strain structure. Because the ground state crystal is highly anharmonic, we find that the cubic structure also has a large Grüneisen parameter (compared to the highly harmonic silicon, which has Grüneisen parameters an order of magnitude smaller [67,68]), but is itself an order of magnitude smaller than that of the strained crystal, which is closer to the phase transition. This indicates that if the ground state structure of STO were not centrosymmetric, it would likely be a good electro-optically active material (like BTO). This suggests that alloying with a judiciously chosen element (like barium, to make $Ba_xSr_{1-x}TiO_3$, for example) to break the inversion symmetry may be a way to induce a strong EO response. Our results and the correspondence to large Grüneisen parameters at the critical strain values suggests that large Grüneisen parameters, and therefore large anharmonicity, in non-centrosymmetric crystals could indicate large EO responses. However, depending on the symmetry of the crystal and the size of the unit cell, the calculation of the full Grüneisen tensor can be resource intensive. We therefore calculate the Grüneisen parameter of the strained STO crystal, approximating it as isotropic. This is not unreasonable approximation as the c/a ratio at the critical strain is 1.02, which is very nearly cubic. The calculated Grüneisen parameters are listed in Table 3. They exhibit the same trends we saw in the full calculation of the Grüneisen tensor, in that the magnitude of the parameter increases as the strain approaches the critical strain. We can also compare the parameter with the average of the tensor components, and we see very good agreement at -1.0% strain and reasonable agreement at -1.2% strain. Therefore, the isotropic Grüneisen parameter could provide a quick way to screen materials for potential large EO responses with less cost than calculating the full tensor or the full EO response itself.

Other simple models besides the isotropic Grüneisen parameter that can serve as a proxy are also of value. Consider a 1-D oscillator model of the Pockels effect. This can be written as an oscillator with an anharmonic contribution to the force and damping, with driving optical and static electric fields:

$$\ddot{x} + \Gamma\dot{x} + \omega_0^2 x + \upsilon x^2 = \left(\frac{e}{m}\right)[E(\omega,t) + \beta E(0)], \tag{10}$$

where the coefficient Γ is the damping constant, υ is the anharmonic force constant, e is the electric charge, m the electron mass, β is a local field parameter given by $(\epsilon^0 + 2)/3$, and $E(\omega,t)$ and $E(0)$ are external optical and static electric fields, respectively. This model was analyzed by Kurtz and Robinson [69], who showed that the Pockels "tensor" (a single coefficient in this 1-D model) is directly proportional to the magnitude of the anharmonic force constant. In this spirit, we displaced the atoms in the STO unit cell from their equilibrium positions according

8

to the eigenvector of the first optical phonon mode, calculated the force on the titanium atom in that direction, and fit it to a simple oscillator with an anharmonic force in order to extract the anharmonic force constant. A schematic diagram of this model is shown in Figure 6. The results of doing so are presented in Table 4. The resulting anharmonic force constants are largest for the 0.0% strain case and for the critical -1.2% strain case, while being lower for the paraelectric, -1.0% case. This suggests two things: first, that this simplified model can be used to quickly screen anharmonic, non-centrosymmetric materials for EO responses, and second, it reinforces the notion that the anharmonicity in the crystal is the driving force behind the large EO response we see here. For comparison, we perform the same analysis for bulk silicon, which is a very harmonic crystal compared to STO (as evidenced by their thermal expansion coefficients of $\alpha = 2.93 \times 10^{-6}\ \mathrm{K}^{-1}$ [70] for silicon and $\alpha = 32.3 \times 10^{-6}\ \mathrm{K}^{-1}$ for STO [71]). Indeed, the anharmonic force constant in this model in silicon (also listed in Table 3) is much smaller than the constant for STO at any strain.

Finally, a similar theoretical study was performed by Fredrickson *et al* [19], but for BTO instead of STO. Their study was done using the experimental lattice parameters for BTO. Despite this difference, they also predict large peaks in the EO response for certain critical strains that are associated with soft phonon modes. This may suggest that enhancement in the EO response under strain is a general feature of non-centrosymmetric perovskite crystals, but further study is needed before such a statement can be made with certainty.

Conclusions

Under both tensile and compressive biaxial strain, we calculate the EO response of STO. At certain critical values of strain, the response is significantly enhanced, and this enhancement is shown to be associated with the onset of a FE phase transition driven by a softening phonon mode. We relate this to the anharmonicity in the titanium-oxygen bonds using theoretically calculated Grüneisen tensor and illustrate this effect with a simplified 1-D model. A similar result is predicted for BTO [19], which suggests that enhancement of the EO response under strain is a characteristic of materials where strain may result in the onset of an appropriate structural phase transition. The magnitude of the enhanced EO response we predict in strained STO is comparable to the EO response of BTO thin films, which is among the largest known experimentally. Our work suggests that STO can be useful in silicon photonics if it can be grown under a sufficient amount of strain.

Acknowledgements

References

[1]   G. T. Reed, G. Mashanovich, F. Y. Gardes, and D. J. Thomson, Nat. Photonics **4**, 518 (2010).

[2]   M. J. R. Heck, H.-W. Chen, A. W. Fang, B. R. Koch, D. Liang, H. Park, M. N. Sysak, and J. E. Bowers, IEEE J. Sel. Top. Quantum Electron. **17**, 333 (2011).

[3]   J. Gourlay, M. Forbes, and M. Desmulliez, Electron. Commun. Eng. J. **13**, 221 (2001).

[4]   A. F. Benner, M. Ignatowski, J. A. Kash, D. M. Kuchta, and M. B. Ritter, IBM J. Res. Dev. **49**, 755 (2005).

[5]   A. Melikyan, L. Alloatti, A. Muslija, D. Hillerkuss, P. C. Schindler, J. Li, R. Palmer, D. Korn, S. Muehlbrandt, D. Van Thourhout, B. Chen, R. Dinu, M. Sommer, C. Koos, M. Kohl, W. Freude, and J. Leuthold, Nat. Photonics **8**, 229 (2014).

[6]   K. Yamada, Y. Urino, T. Nakamura, and Y. Arakawa, NTT Tech. Rev. **11**, (2013).

[7]   F. Eltes, D. Caimi, F. Fallegger, M. Sousa, E. O'Connor, M. D. Rossell, B. Offrein, J. Fompeyrine, and S. Abel, ACS Photonics **3**, 1698 (2016).

[8]   L. Alloatti, R. Palmer, S. Diebold, K. P. Pahl, B. Chen, R. Dinu, M. Fournier, J. M. Fedeli, T. Zwick, W. Freude, C. Koos, and J. Leuthold, Light Sci. Appl. **3**, 5 (2014).

[9]   R. S. Jacobsen, K. N. Andersen, P. I. Borel, J. Fage-Pedersen, L. H. Frandsen, O. Hansen, M. Kristensen, A. V. Lavrinenko, G. Moulin, H. Ou, C. Peucheret, B. Zsigri, and A. Bjarklev, Nature **441**, 199 (2006).

[10]   C. L. Manganelli, P. Pintus, and C. Bonati, Opt. Express **23**, 28649 (2015).

[11]   K. J. Kormondy, Y. Popoff, M. Sousa, F. Eltes, D. Caimi, M. D. Rossell, M. Fiebig, P. Hoffmann, C. Marchiori, M. Reinke, M. Trassin, A. A. Demkov, J. Fompeyrine, and S. Abel, Nanotechnology **28**, 075706 (2017).

[12]   S. Abel, T. Stoferle, C. Marchiori, D. Caimi, L. Czornomaz, M. Stuckelberger, M. Sousa, B. J. Offrein, and J. Fompeyrine, J. Light. Technol. **34**, 1688 (2016).

[13]   S. Abel, T. Stöferle, C. Marchiori, C. Rossel, M. D. Rossell, R. Erni, D. Caimi, M. Sousa, A. Chelnokov, B. J. Offrein, and J. Fompeyrine, Nat. Commun. **4**, 1671 (2013).

[14]   E. L. Wooten, K. M. Kissa, A. Yi-Yan, E. J. Murphy, D. a. Lafaw, P. F. Hallemeier, D. Maack, D. V. Attanasio, D. J. Fritz, G. J. McBrien, and D. E. Bossi, IEEE J. Sel. Top. Quantum Electron. **6**, 69 (2000).

[15]   D. Janner, D. Tulli, M. Garcia-Granda, M. Belmonte, and V. Pruneri, Laser Photonics Rev. **3**, 301 (2009).

[16]   R. Boyd, *Nonlinear Optics*, 3rd ed. (Academic Press, 2008).

[17]   C. Xiong, W. H. P. Pernice, J. H. Ngai, J. W. Reiner, D. Kumah, F. J. Walker, C. H. Ahn, and H. X. Tang, Nano Lett. **14**, 1419 (2014).

[18]   M. Veithen, X. Gonze, and P. Ghosez, Phys. Rev. Lett. **93**, 1 (2004).

[19] K. D. Fredrickson, V. V. Vogler-Neuling, K. J. Kormondy, D. Caimi, F. Eltes, M. Sousa, J. Fompeyrine, S. Abel, and A. A. Demkov, Phys. Rev. B **98**, 075136 (2018).

[20] R. A. McKee, F. J. Walker, and M. F. Chisholm, Phys. Rev. Lett. **81**, 3014 (1998).

[21] C. Dubourdieu, J. Bruley, T. M. Arruda, A. Posadas, J. Jordan-Sweet, M. M. Frank, E. Cartier, D. J. Frank, S. V. Kalinin, A. A. Demkov, and V. Narayanan, Nat. Nanotechnol. **8**, 748 (2013).

[22] K. J. Kormondy, S. Abel, F. Fallegger, Y. Popoff, P. Ponath, A. B. Posadas, M. Sousa, D. Caimi, H. Siegwart, E. Uccelli, L. Czornomaz, C. Marchiori, J. Fompeyrine, and A. A. Demkov, Microelectron. Eng. **147**, 215 (2015).

[23] B. W. Wessels, Annu. Rev. Mater. Res. **37**, 659 (2007).

[24] H. Unoki and T. Sakudo, J. Phys. Soc. Japan **23**, 546 (1967).

[25] P. A. Fleury, J. F. Scott, and J. M. Worlock, Phys. Rev. Lett. **21**, 16 (1968).

[26] G. Shirane and Y. Yamada, Phys. Rev. **177**, 858 (1969).

[27] T. Mitsui and W. B. Westphal, Phys. Rev. **124**, 1354 (1961).

[28] T. Sakudo and H. Unoki, Phys. Rev. Lett. **26**, 851 (1971).

[29] R. Viana, P. Lunkenheimer, J. Hemberger, R. Böhmer, and A. Loidl, Phys. Rev. B **50**, 601 (1994).

[30] K. A. Müller and H. Burkard, Phys. Rev. B **19**, 3593 (1979).

[31] N. A. Pertsev, A. K. Tagantsev, and N. Setter, Phys. Rev. B **61**, R825 (2000).

[32] N. A. Pertsev, A. K. Tagantsev, and N. Setter, Phys. Rev. B **65**, 219901 (2002).

[33] N. Sai and D. Vanderbilt, Phys. Rev. B **62**, 13942 (2000).

[34] A. A. Demkov, A. B. Posadas, H. Seo, M. Choi, K. J. Kormondy, P. Ponath, R. C. Hatch, M. D. McDaniel, T. Q. Ngo, and J. G. Ekerdt, ECS Trans. **54**, 255 (2013).

[35] M. Choi, A. Posadas, R. Dargis, C.-K. Shih, A. A. Demkov, D. H. Triyoso, N. David Theodore, C. Dubourdieu, J. Bruley, and J. Jordan-Sweet, J. Appl. Phys. **111**, 064112 (2012).

[36] X. F. Wang, J. Wang, Q. Li, M. S. Moreno, X. Y. Zhou, J. Y. Dai, Y. Wang, and D. Tang, J. Phys. D. Appl. Phys. **42**, 085409 (2009).

[37] X. Hu, H. Li, Y. Liang, Y. Wei, Z. Yu, D. Marshall, J. Edwards, R. Droopad, X. Zhang, A. A. Demkov, K. Moore, and J. Kulik, Appl. Phys. Lett. **82**, 203 (2003).

[38] J. Ramdani, R. Droopad, Z. Yu, J. . Curless, C. . Overgaard, J. Finder, K. Eisenbeiser, J. . Hallmark, W. . Ooms, V. Kaushik, P. Alluri, and S. Pietambaram, Appl. Surf. Sci. **159–160**, 127 (2000).

[39] C. J. Först, C. R. Ashman, K. Schwarz, and P. E. Blöchl, Nature **427**, 53 (2004).

[40] H. Li, X. Hu, Y. Wei, Z. Yu, X. Zhang, R. Droopad, A. A. Demkov, J. Edwards, K. Moore, W. Ooms, J. Kulik, and P. Fejes, J. Appl. Phys. **93**, 4521 (2003).

[41] C. Dubourdieu, I. Gelard, O. Salicio, G. Saint Girons, B. Vilquin, and G. Hollinger, Int. J. Nanotechnol. **7**, 320 (2010).

[42] N. A. Pertsev, A. G. Zembilgotov, and A. K. Tagantsev, Phys. Rev. Lett. **80**, 1988 (1998).

[43] A. Antons, J. B. Neaton, K. M. Rabe, and D. Vanderbilt, Phys. Rev. B **71**, 024102 (2005).

[44] S. Hyun and K. Char, Appl. Phys. Lett. **79**, 254 (2001).

[45] H. Ma, J. Levy, M. D. Biegalski, S. Trolier-McKinstry, and D. G. Schlom, J. Appl. Phys. **105**, 014102 (2009).

[46] W. Peng, R. Tétot, G. Niu, E. Amzallag, B. Vilquin, J.-B. Brubach, and P. Roy, Sci. Rep. **7**, 2160 (2017).

[47] M. Veithen, X. Gonze, and P. Ghosez, Phys. Rev. B **71**, 125107 (2005).

[48] X. Gonze, Phys. Rev. B **55**, 10337 (1997).

[49] X. Gonze and C. Lee, Phys. Rev. B **55**, 10355 (1997).

[50] M. C. Robinson and A. C. H. Hallett, Can. J. Phys. **44**, 2211 (1966).

[51] M. R. Stuart, J. Appl. Phys. **26**, 1399 (1955).

[52] X. Gonze, Zeitschrift Für Krist. - Cryst. Mater. **220**, 558 (2005).

[53] X. Gonze, B. Amadon, P.-M. Anglade, J.-M. Beuken, F. Bottin, P. Boulanger, F. Bruneval, D. Caliste, R. Caracas, M. Côté, T. Deutsch, L. Genovese, P. Ghosez, M. Giantomassi, S. Goedecker, D. R. Hamann, P. Hermet, F. Jollet, G. Jomard, S. Leroux, M. Mancini, S. Mazevet, M. J. T. Oliveira, G. Onida, Y. Pouillon, T. Rangel, G.-M. Rignanese, D. Sangalli, R. Shaltaf, M. Torrent, M. J. Verstraete, G. Zerah, and J. W. Zwanziger, Comput. Phys. Commun. **180**, 2582 (2009).

[54] X. Gonze, F. Jollet, F. Abreu Araujo, D. Adams, B. Amadon, T. Applencourt, C. Audouze, J.-M. Beuken, J. Bieder, A. Bokhanchuk, E. Bousquet, F. Bruneval, D. Caliste, M. Côté, F. Dahm, F. Da Pieve, M. Delaveau, M. Di Gennaro, B. Dorado, C. Espejo, G. Geneste, L. Genovese, A. Gerossier, M. Giantomassi, Y. Gillet, D. R. Hamann, L. He, G. Jomard, J. Laflamme Janssen, S. Le Roux, A. Levitt, A. Lherbier, F. Liu, I. Lukačević, A. Martin, C. Martins, M. J. T. Oliveira, S. Poncé, Y. Pouillon, T. Rangel, G.-M. Rignanese, A. H. Romero, B. Rousseau, O. Rubel, A. A. Shukri, M. Stankovski, M. Torrent, M. J. Van Setten, B. Van Troeye, M. J. Verstraete, D. Waroquiers, J. Wiktor, B. Xu, A. Zhou, and J. W. Zwanziger, Comput. Phys. Commun. **205**, 106 (2016).

[55] D. R. Hamann, X. Wu, K. M. Rabe, and D. Vanderbilt, Phys. Rev. B - Condens. Matter Mater. Phys. **71**, (2005).

[56] M. Teter, Phys. Rev. B **48**, 5031 (1993).

[57] D. M. Ceperley and B. J. Alder, Phys. Rev. Lett. **45**, 566 (1980).

13

[58]   J. P. Perdew and A. Zunger, Phys. Rev. B **23**, 5048 (1981).

[59]   H. J. Monkhorst and J. D. Pack, Phys. Rev. B **13**, 5188 (1976).

[60]   Y. A. Abramov, V. G. Tsirelson, V. E. Zavodnik, S. A. Ivanov, and Brown I. D., Acta Crystallogr. Sect. B Struct. Sci. **51**, 942 (1995).

[61]   J. F. Nye, *Physical Properties of Crystals* (Oxford University Press, 1985).

[62]   J. W. Zwanziger, J. Galbraith, Y. Kipouros, M. Torrent, M. Giantomassi, and X. Gonze, Comput. Mater. Sci. **58**, 113 (2012).

[63]   A. G. Beattie and G. A. Samara, J. Appl. Phys. **42**, 2376 (1971).

[64]   K. Brugger, Phys. Rev. **137**, A1826 (1965).

[65]   R. E. Cohen and H. Krakauer, Ferroelectrics **136**, 65 (1992).

[66]   M. Zgonik, P. Bernasconi, M. Duelli, R. Schlesser, P. Günter, M. H. Garrett, D. Rytz, Y. Zhu, and X. Wu, Phys. Rev. B **50**, 5941 (1994).

[67]   W. B. Gauster, Phys. Rev. B **4**, 1288 (1971).

[68]   J. Prechtel, J. Kalus, E. Lüscher, L. Pintschovius, and R. Ghosh, Phys. Status Solidi **93**, 653 (1979).

[69]   S. K. Kurtz and F. N. H. Robinson, Appl. Phys. Lett. **10**, 62 (1967).

[70]   O. Madelung, *Semiconductors: Data Handbook* (Springer Berlin Heidelberg, Berlin, Heidelberg, 2004).

[71]   D. de Ligny and P. Richet, Phys. Rev. B **53**, 3013 (1996).

Figures

Figure 1
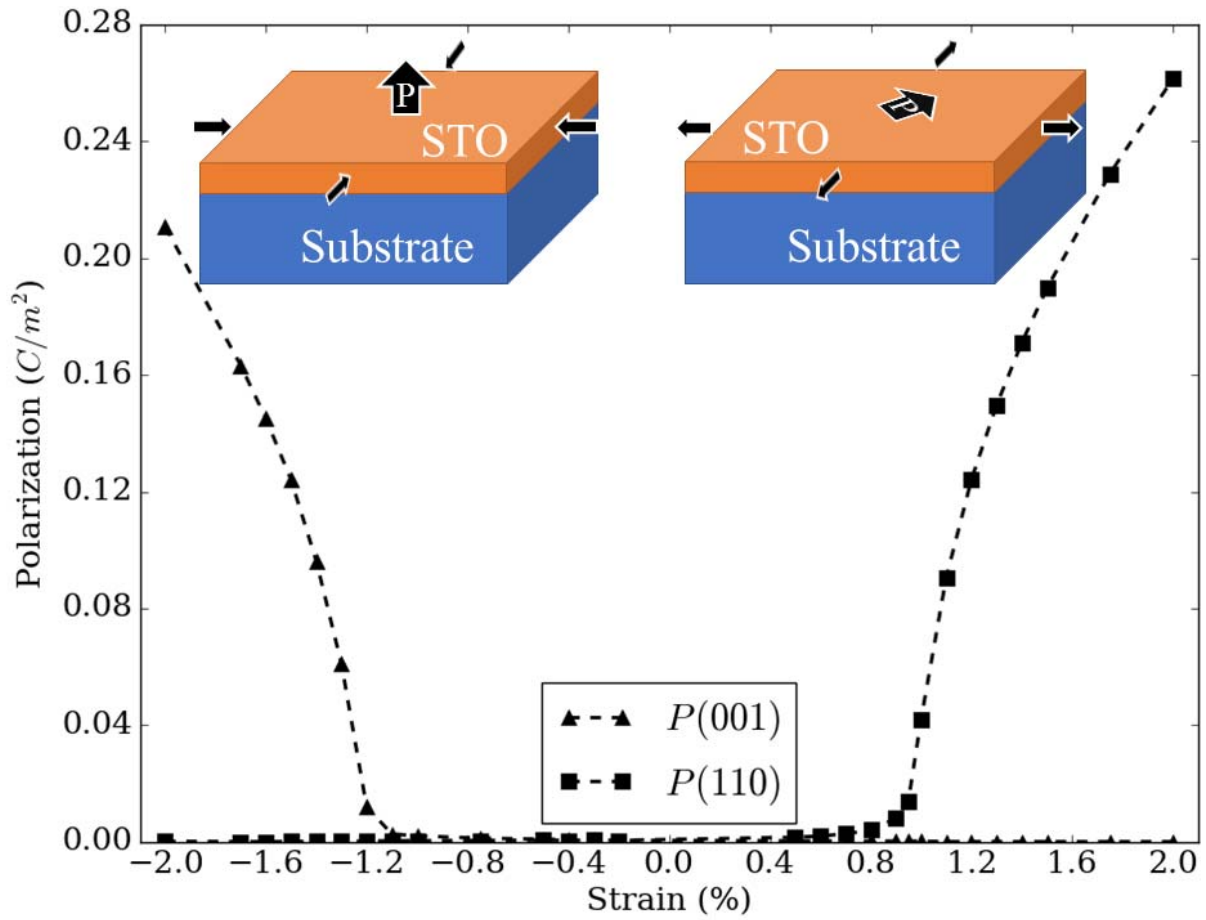
Figure 1: The magnitude of the polarization in STO as a function of strain. The onset of the polarization and the ferroelectric phase transition and displacement of the titanium ion in the (001) and the (110) directions occurs at -1.2% and 1.0% strain, respectively.

Figure 2
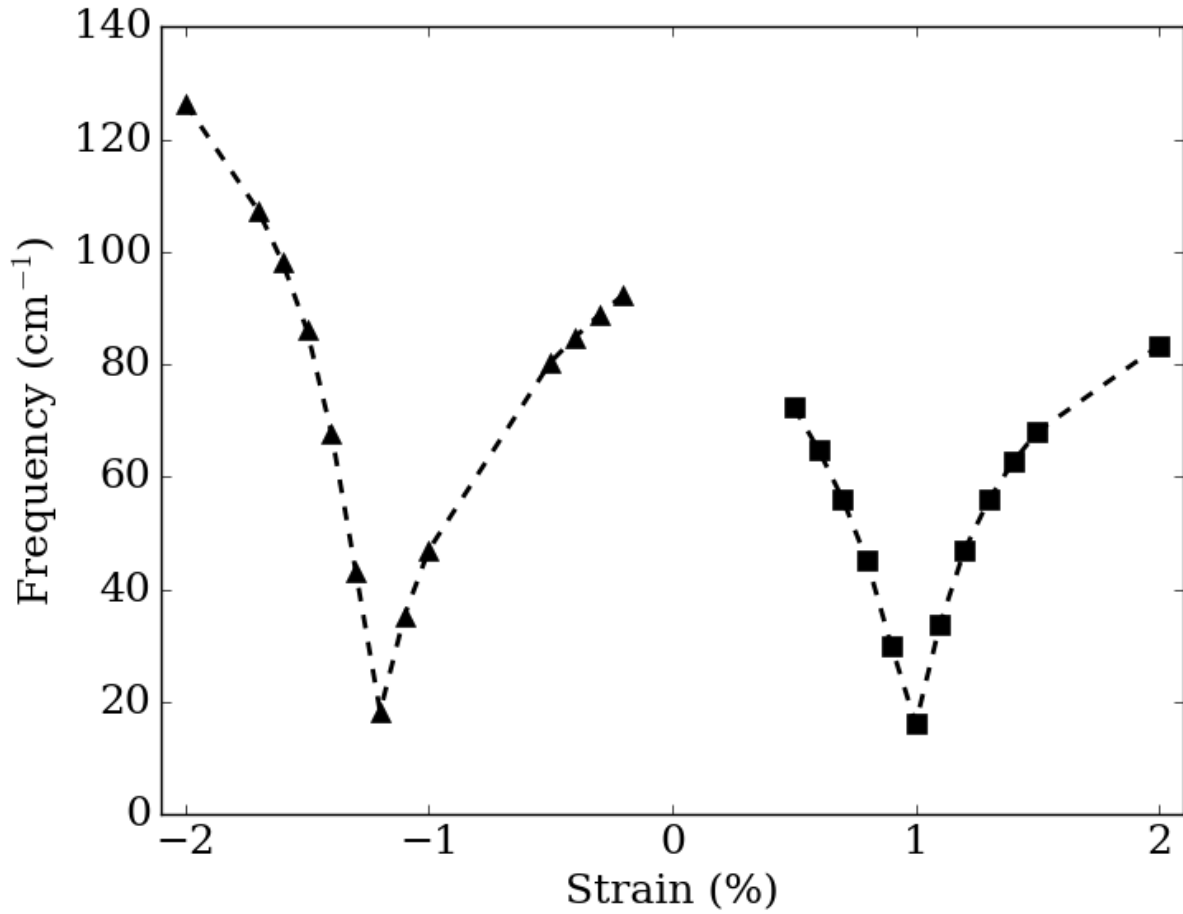
Figure 2: Frequency of the first optical mode of STO as a function of strain. The mode is in the (001) direction under compressive strain (triangular markers) and in the (110) direction under tensile strain (square markers). The mode goes soft at -1.2% and at 1.0% strain, corresponding to the ferroelectric phase transition and the divergence in the EO response.

Figure 3
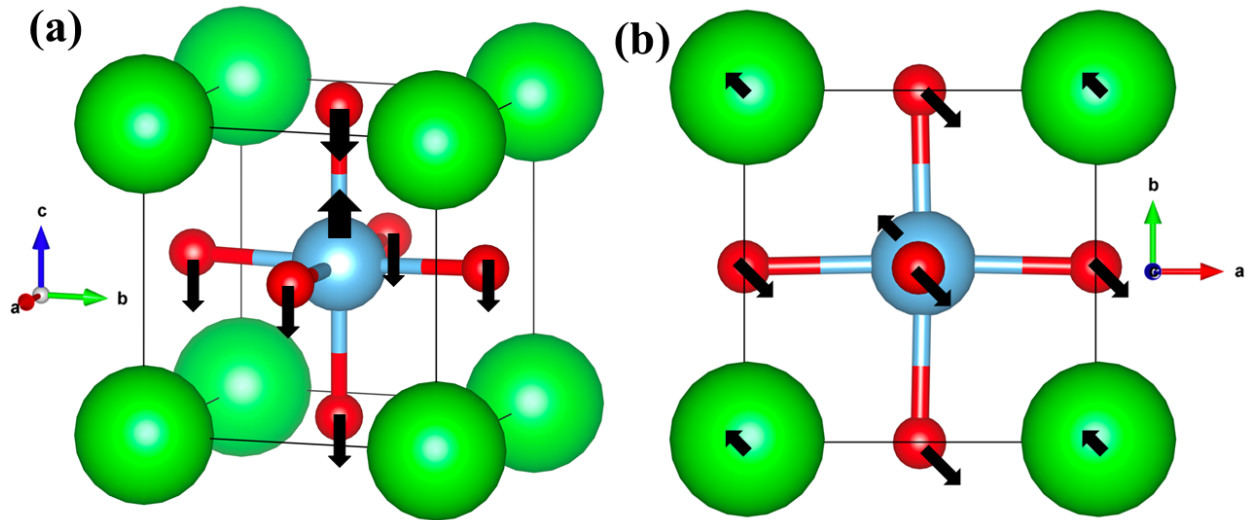
Figure 3: The displacement patterns of the first optical mode which goes soft and drives the structural phase transition. The strontium ions are colored green, the titanium ions blue, and the oxygen ions red. (a) The displacement pattern for the soft mode for compressive strain is shown here. The titanium ion moves in the (001) direction and the oxygen ions move in the opposite direction. The strontium ion moves in the same direction as the titanium ion, but its displacement is an order of magnitude smaller, so we do not label it here. (b) The displacement pattern for the soft mode under tensile strain is shown here along the $(00\bar{1})$-direction. The titanium and strontium ions move in the $(\bar{1}10)$ direction and the oxygen ions move in the $(1\bar{1}0)$ direction.

Figure 4
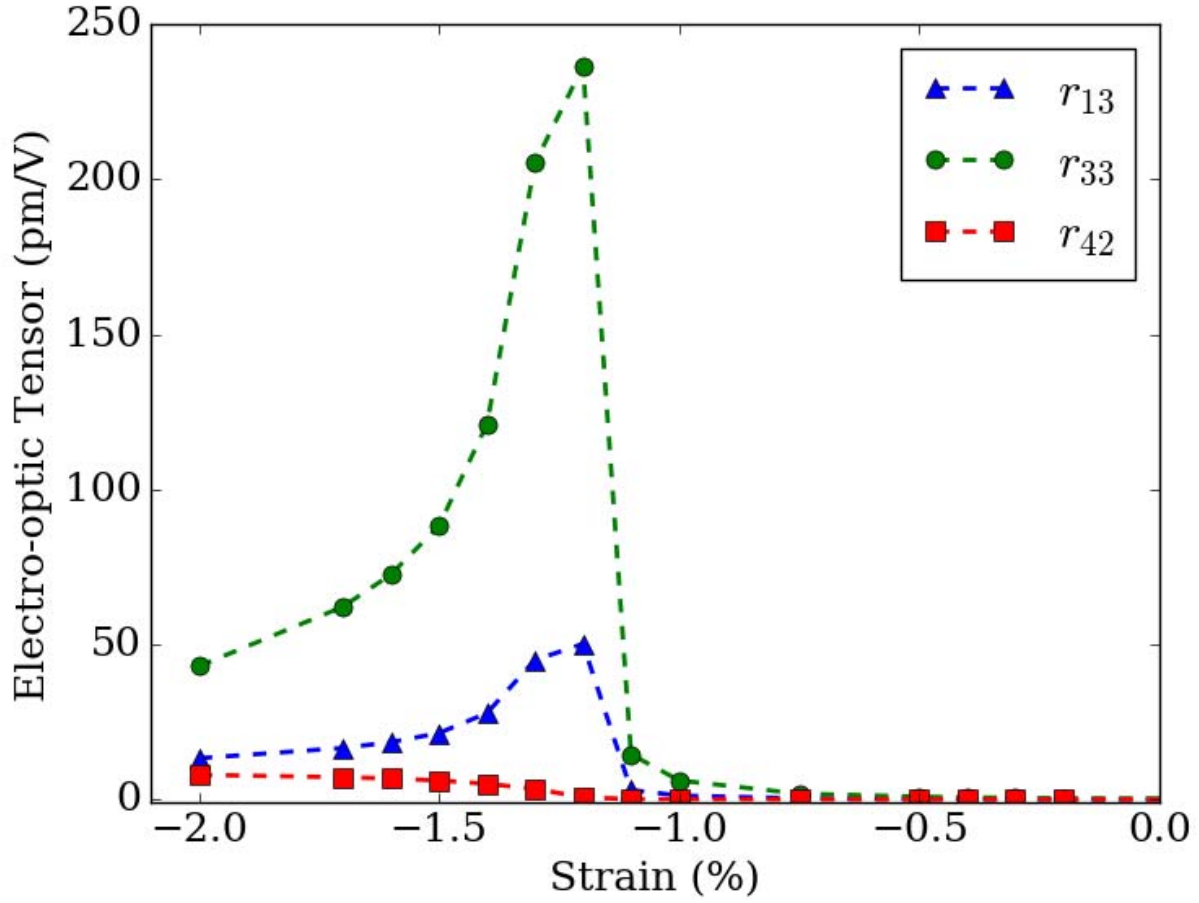
Figure 4: The magnitudes of the largest EO tensor components for STO under compressive strain. The EO response peaks at -1.20% strain.

Figure 5
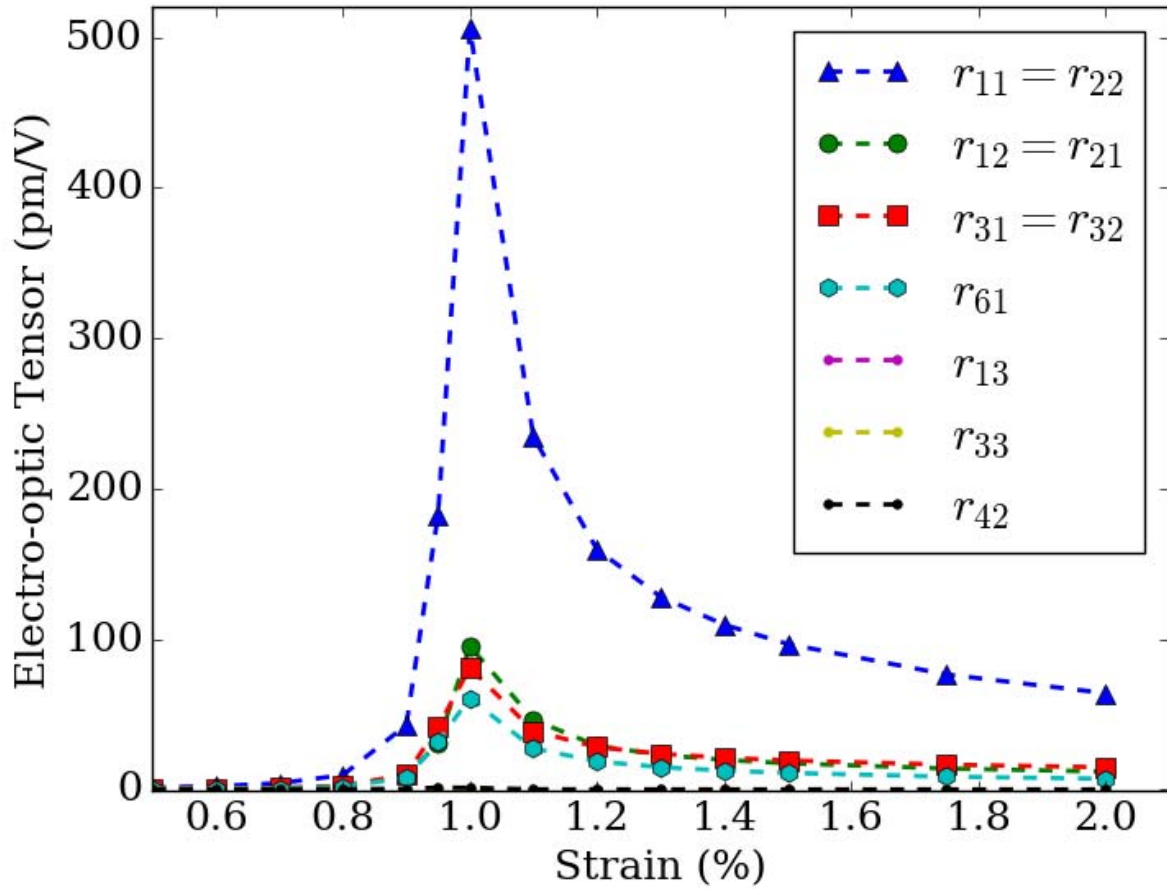
Figure 5: The magnitudes of the largest EO tensor components under tensile strain. The EO response peaks at 1.00% strain.

Figure 6
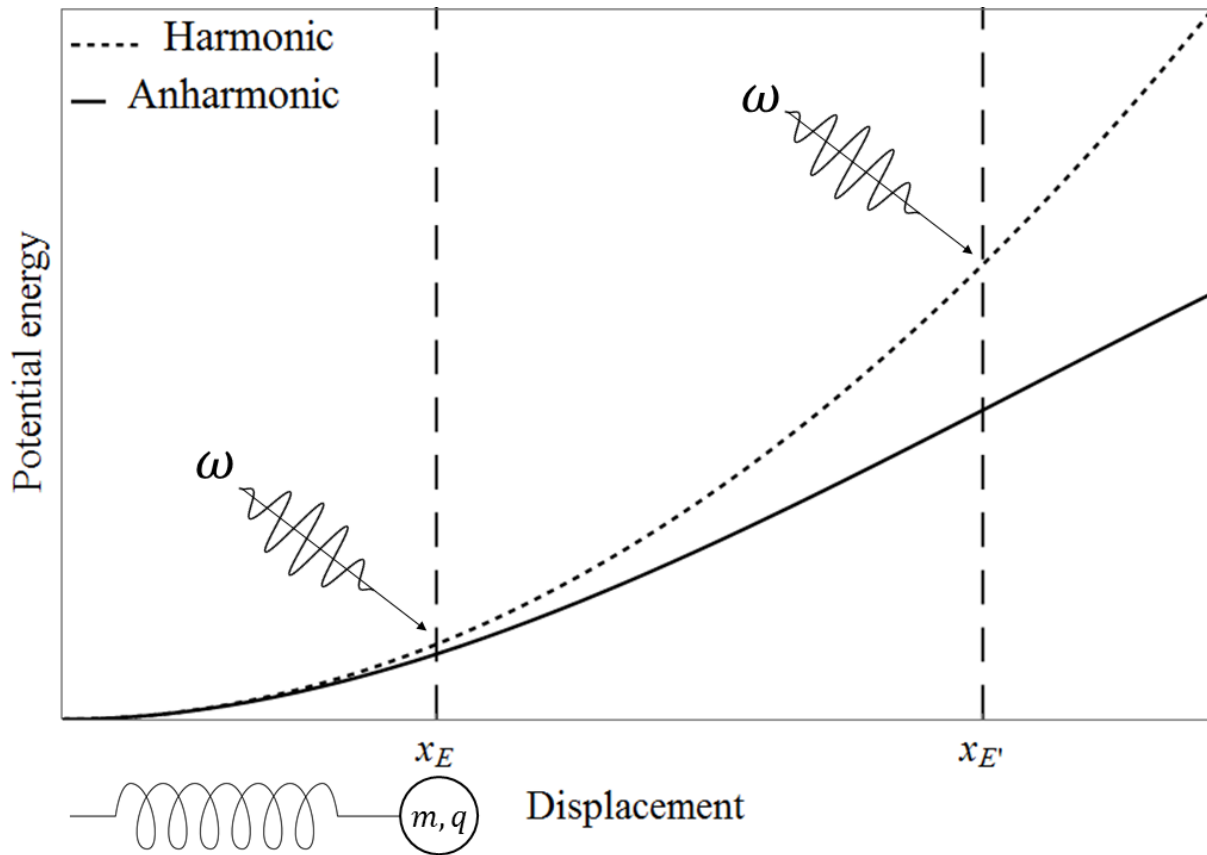
Figure 6: A schematic diagram of the 1-D oscillator model we use to illustrate the importance of anharmonicity in the crystal for the EO response. For an applied external electric field E, the equilibrium position of the oscillator shifts to x_E. Similarly, for an external field E', the equilibrium position shifts to $x_{E'}$. The resonant frequency of the oscillator, $\omega_0 = \sqrt{k/m}$, does not change with applied external field for a harmonic potential, but it does for the anharmonic potential.

Tables

Table 1: The largest converse piezoelectric effect contributions to the Pockels tensor at two compressive strains, and a comparison of their magnitudes to that of the clamped Pockels tensor. The converse piezoelectric effect has a relatively small contribution when compared to the clamped contribution and can safely be neglected.

Strain	Largest r_{ij}^{piezo} Component (pm/V)	Fraction of Largest r_{ij}^{η} Component
-1.0%	$r_{33}^{\text{piezo}} = -0.47$	$r_{33}^{\text{piezo}}/r_{33}^{\eta} = 0.076$
-1.2%	$r_{33}^{\text{piezo}} = -28.90$	$r_{33}^{\text{piezo}}/r_{33}^{\eta} = 0.122$

Table 2: Non-zero components of the anisotropic Grüneisen tensor of the first optical mode for the ground state, cubic structure and for two structures under compressive, in-plane strain. The Grüneisen parameter for this mode is largest at the strain at which the mode is softest, and at which the EO response diverges. The average of the components is also included for comparison with the isotropic case. Note that we do not label the polarization as it is in the (001)-direction for the strained cases.

Strain	$\gamma_{11} = \gamma_{22}$	γ_{33}	γ_{avg}
0.0%	12.3	12.3	12.3
-1.0%	-39.0	237.9	53.3
-1.2%	-78.0	825.0	223.0

Table 3: Isotropic Grüneisen parameter of the first optical mode for the ground state, cubic structure and for two structures under compressive, in-plane strain. The Grüneisen parameter for this mode is largest at the strain at which the mode is softest, and at which the EO response diverges.

Strain	Grüneisen Parameter
0.0%	12.3
-1.0%	53.8
-1.2%	172.2

Table 4: Anharmonic force coefficient in a simplified 1-D model of the phonon mode driving the EO response. The larger magnitudes are indicative of greater anharmonicity. For comparison, we applied the same approach to silicon, which is well known to be harmonic. The anharmonic contribution is much smaller than in STO.

Material	Strain	υ (Bohr^{-1} s^{-2})
	0.0%	-0.59
STO	-1.0%	-0.50
	-1.2%	-0.59
Silicon	0.0%	0.04